Pattern Formation in an RD-MCNN with Locally Active Memristors

(Article begins on next page)

19 October 2024

We are IntechOpen,
the world's leading publisher of
Open Access books
Built by scientists, for scientists

5,500
Open access books available

135,000
International authors and editors

165M
Downloads

Our authors are among the

154
Countries delivered to

TOP 1%
most cited scientists

12.2%
Contributors from top 500 universities

Interested in publishing with us?
Contact book.department@intechopen.com

Chapter

Pattern Formation in a RD-MCNN with Locally Active Memristors

Ahmet Samil Demirkol, Alon Ascoli, Ioannis Messaris and Ronald Tetzlaff

Abstract

This chapter presents the mathematical investigation of the emergence of static patterns in a Reaction–Diffusion Memristor Cellular Nonlinear Network (RD-MCNN) structure *via* the application of the theory of local activity. The proposed RD-MCNN has a planar grid structure, which consists of identical memristive cells, and the couplings are established in a purely resistive fashion. The single cell has a compact design being composed of a locally active memristor in parallel with a capacitor, besides the bias circuitry, namely a DC voltage source and its series resistor. We first introduce the mathematical model of the locally active memristor and then study the main characteristics of its AC equivalent circuit. Later on, we perform a stability analysis to obtain the stability criteria for the single cell. Consequently, we apply the theory of local activity to extract the parameter space associated with locally active, edge-of-chaos, and sharp-edge-of-chaos domains, performing all the necessary calculations parametrically. The corresponding parameter space domains are represented in terms of intrinsic cell characteristics such as the DC operating point, the capacitance, and the coupling resistance. Finally, we simulate the proposed RD-MCNN structure where we demonstrate the emergence of pattern formation for various values of the design parameters.

Keywords: pattern formation, memristor, reaction–diffusion, cellular nonlinear networks, destabilization, local activity, complexity

1. Introduction

An important feature of complex systems is the emergence of spatiotemporal patterns, which can be observed in numerous physical systems consisting of homogeneous media [1]. Among many examples, the emergence phenomenon can occur as a result of oscillatory kinetics in a chemical reaction [2], self-organization of biological organisms [3], mechanical vibration on liquid surfaces [4], or mineral precipitation on geologic surfaces [5]. In particular, network dynamics of pattern formation is considered to be the key attribute of information processing and memory storage in biological neural networks [6] and, hence, is the main concern in neuroscience. Following the consequences of the seminal paper of Turing [7] where he introduced the chemical basis of morphogenesis, the mechanism behind pattern formation dynamics has been extensively studied in various scientific branches. On one hand, different mathematical models have been proposed to elucidate the analytical principles of pattern formation dynamics [8]. On the other hand, there

has been an ambiguity on the conceptual definition of the complexity phenomenon, which was previously described as symmetry breaking, instability of the homogenous, exchange of energy, or self-organization. In [9], Chua has proposed the theory of local activity, as the origin of complexity, where he quantitatively defined the mathematical principle behind the emergence of complex patterns in a homogenous medium. In this way, the theory of local activity assembled various definitions under the same framework and enabled the quantitative investigation of pattern formation dynamics, especially through electrical circuits. Since then, several works dealing with pattern formation dynamics on electrical hardware have referred to the theory of local activity to perform robust and quantitative analysis (e.g., see [10]). Mathematically, a well-known method to realize pattern formation dynamics is to implement reaction–diffusion partial differential equations (RD-PDEs) [11]. Various physical systems adopting reaction–diffusion equations have been shown to create well-known spatiotemporal phenomena such as traveling waves or clustering patterns [12]. Therefore, circuit implementations of RD-PDEs would be a reasonable approach to capture pattern formation dynamics on electrical hardware. Cellular nonlinear networks (CNNs), which can be described as homogeneous structures composed of evenly spaced and locally coupled identical cells, are prominent hardware solutions to implement the RD-PDEs. In particular, the reaction dynamics of an RD-PDE can be implemented by the identical cells of a CNN, while the diffusive dynamics of the same RD-PDE can be successfully discretized using the central difference approach and then implemented *via* resistive coupling between the identical neighboring cells, resulting in the so-called RD-CNN structure [13]. Motivated by this approach, emergent phenomena, such as Turing patterns or auto waves, have already been demonstrated across RD-CNNs [14].

The high-speed data transfer capability of modern mobile communication systems has led to the introduction of 5G and, in the future, 6G networks successively in a short period, which has enabled a new era in technology such as Industry 4.0 and Internet-of-Things (IoT) [15]. In parallel with the requirements of the new technological applications and the performance criteria of the corresponding hardware realizations, the design of bio-inspired neuromorphic systems utilizing the in-memory-computing principle, which stands as an alternative option to the design of conventional von-Neumann computing architectures where memory and processor units are separated from each other, has recently gained a lot of attention [16]. Similarly, there is a huge research effort in academia and industry for developing efficient fabrication techniques to implement the new in-memory computing circuit elements such as resistive switching memories, which can apparently be described as memristors [17]. The memristor, a two-terminal circuit element that was theoretically hypothesized 50 years ago, can be briefly considered as a nonlinear resistor with inherent memory dynamics [18]. Due to recent developments in physical implementations of different types of memory devices, the modeling and analysis of memristors and memristive systems have also gained attention, resulting in comprehensive circuit and system theoretical investigations [19]. Accordingly, the availability of manufactured nanoscale memristors emerges as a key enabler for the implementation of memory and processing units realized in the same place of compact hardware, and thus, provides the opportunity to design novel bio-inspired systems with in-memory-computing capabilities. In this way, it can be possible to overcome the end of Moore's law by engineering the information processing architectures, rather than downscaling the semiconductor device dimensions, which practically has come to an end.

Consistent with the above-mentioned text, locally active memristors have already been utilized in the design and application of spiking neural cells

demonstrating promising results [20], while prominent artificial neural network designs employing memristor crossbar arrays have been presented in several works [21]. Besides, the theory of memristor cellular nonlinear networks (MCNNs) has been comprehensively investigated in [22–25] and the formation of Turing patterns with reaction–diffusion MCNNs (RD-MCNNs) has been introduced in [26]. In addition, pattern formation utilizing locally active NbO memristors in an MCNN has been presented in [27]. In a previous work [28], we have presented the model-based analytical investigation of dynamic pattern formation in a RD-MCNN, exploiting a manufactured locally active memristor, while the proposed single cell structure, as well as the subsequent results, is different from those presented here. Similarly, in [29], we have presented preliminary results of the mathematical investigation of static pattern formation in a RD-MCNN structure. The goal of this work is to extend the content of the previously presented works and to introduce an analytical design procedure for the implementation of static pattern formation across a compact RD-MCNN structure while taking into account the theory of local activity for the mathematical treatment. To enable the locally active dynamics, we employ a nanoscale locally active generic memristor model in the design of the basic network cell. The proposed RD-MCNN has a planar grid form and is composed of locally coupled identical cells. The compact unit cell consists of a locally active memristor in parallel with a linear capacitor, besides the bias circuitry, namely a DC voltage source and its series resistor. We first introduce the mathematical definition of the locally active generic memristor employed and, then, study the main characteristics of its AC equivalent circuit. Later on, we perform a quick stability analysis and determine stability criteria for the single cell. Consequently, we apply the theory of local activity in order to extract the parameter space with locally active, edge-of-chaos, and sharp-edge-of-chaos domains, performing all the necessary calculations parametrically. The corresponding parameter space domains are illustrated in terms of intrinsic network characteristics such as the cell DC operating point, the cell capacitance, and the coupling resistance. Essentially, we adopt a circuit theoretical approach, regarding the stability analysis of the single cell and the destabilization process after the coupling is established, which promotes an efficient investigation of the criteria to be derived. Finally, we carry out numerical simulations where we demonstrate the emergence of pattern formation across the proposed RD-MCNN structure for various values of the design parameters.

2. The locally active generic memristor

Nanoscale memristors with locally active (i.e., S-shaped) DC current–voltage (I–V) characteristics have been utilized in the design of oscillatory neuron cells [30, 31]. Furthermore, it was shown in [32–34] that memristor models in a generic form are capable of representing the dynamics of these nanoscale devices accurately. Similarly, in this work, we adopt a simplified generic memristor model to implement locally active dynamics, which helps to reduce the complexity and the simulation time of large-scale networks employing such devices. In addition, the adoption of the generic form enables simplified calculations related to the derivation of the AC model of the device, further promoting the clarification of the results.

2.1 The model definition

We introduce the memristor model equations, namely the I–V relationship in Eq. (1), and the state equation in Eq. (2), where $i_m (v_m)$ is the memristor current

(voltage), R_s is the series resistance, T is the state variable representing the temperature, and $G(T) = g_0 \cdot exp\left(-g_1/T\right)$ is the temperature-dependent memductance function. We would like to note that Eqs. (1) and (2) define a sole memristor core with current $i_{mc} = i_m$ and voltage $v_{mc} = v_m \cdot (1 + R_s \cdot G(T))^{-1}$. The parameter values of the given model employed during the numerical simulations can be found in **Table 1**.

$$i_m = v_m \cdot \frac{G(T)}{1 + R_s \cdot G(T)} = v_{mc} \cdot G(T) \qquad (1)$$

$$C_T \frac{dT}{dt} = v_{mc} \cdot i_m - g_T \cdot (T - T_0) \qquad (2)$$

The S-shaped DC I-V curve under the current sweep and the schematic of the complete device, which can be depicted as the series combination of the core memristor and R_s, are introduced in **Figure 1(a)**. At this point, we would like to point out that the negative differential resistance (NDR) region, which hosts the peculiar dynamics of the locally active memristor, is highlighted with the orange color in **Figure 1(a)**.

2.2 The AC equivalent circuit

Since the small-signal equivalent of the memristor plays an important role during the forthcoming circuit theoretical stability analysis, it is crucial to obtain the AC equivalent circuit of the memristor device. For this purpose, we first derive the small-signal equivalent of the core memristor and then combine it in series with R_s to obtain the AC equivalent circuit of the overall memristor. Essentially, we set $R_s = 0\Omega$ in Eqs. (1) and (2) so that the updated equation set represents the core

g_0/S	g_1/K	R_s/Ω	$C_T/(J \bullet K^{-1})$	$g_T/(W \bullet K^{-1})$	$T_0/(K)$
$5 \cdot 10^{-3}$	1700	200	10^{-14}	$6.67 \cdot 10^{-7}$	300

Table 1.
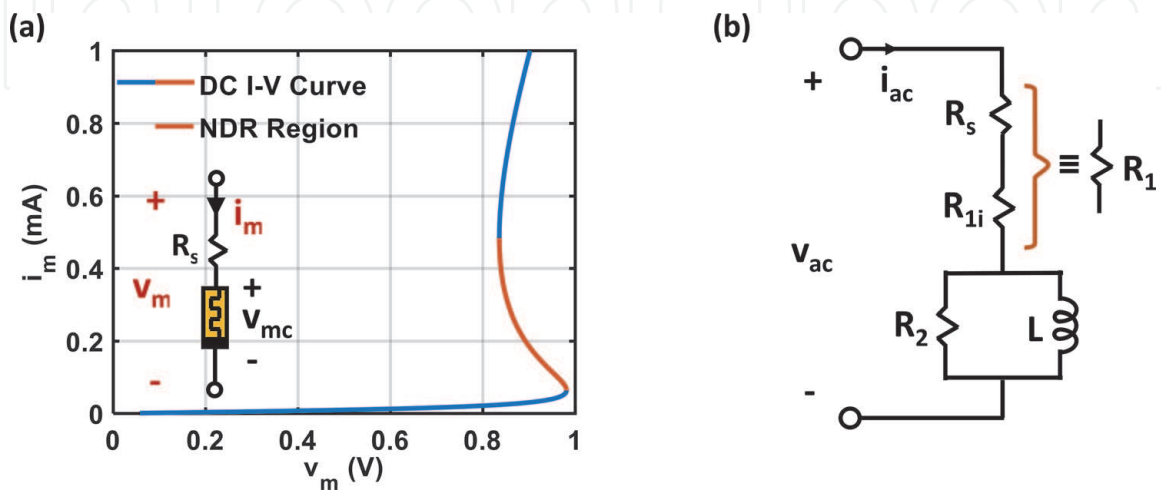*Parameter values for Eqs. (1) and (2).*

Figure 1.
(a) DC I-V curve of the locally active memristor, with NDR region highlighted. The schematic of the memristor, as the series combination between the core device and the series resistor R_s, is depicted in the inset figure. (b) AC equivalent circuit of the entire memristor where $R_1 = R_s + R_{1i}$.

memristor only. Then, we linearize Eqs. (1) and (2) by deriving their first-order Taylor series expansions. As the next step, we apply Laplace transform to the linearized equations, and after a suitable rearrangement of the Laplace equations, we express the impedance function of the core memristor in Foster's first form [35] RL circuit configuration. The final configuration of the AC equivalent circuit of the entire memristor is depicted in **Figure 1(b)**.

Regarding the AC equivalent circuit, R_{1i} represents the inverse of the slope of the DC I-V curve for $R_s = 0\Omega$ and naturally gets negative values in the NDR region. Furthermore, the quantity $(R_{1i} + R_2)$ corresponds to the instantaneous resistance, $V(T_0)/I(T_0)$, of the core memristor, which always gets positive values at a given temperature T_0, since the I-V curve lies either in the first or in the third quadrant. The same explanations are still valid also for $R_s \neq 0\Omega$ if R_{1i} is replaced by $R_1 = R_{1i} + R_s$. Lastly, L represents the dynamics of the core device, while L and R_2 have positive values at all equilibrium points. The graphical representation of the small-signal element values of **Figure 1(b)** versus the DC current I_Q can be found in **Figure 2**, where we use parameter values as given in **Table 1** during the numerical simulations. Finally, a similar procedure regarding the derivation of the AC equivalent circuit of a generic memristor including a detailed investigation and graphical illustration can be found in [36] as well.
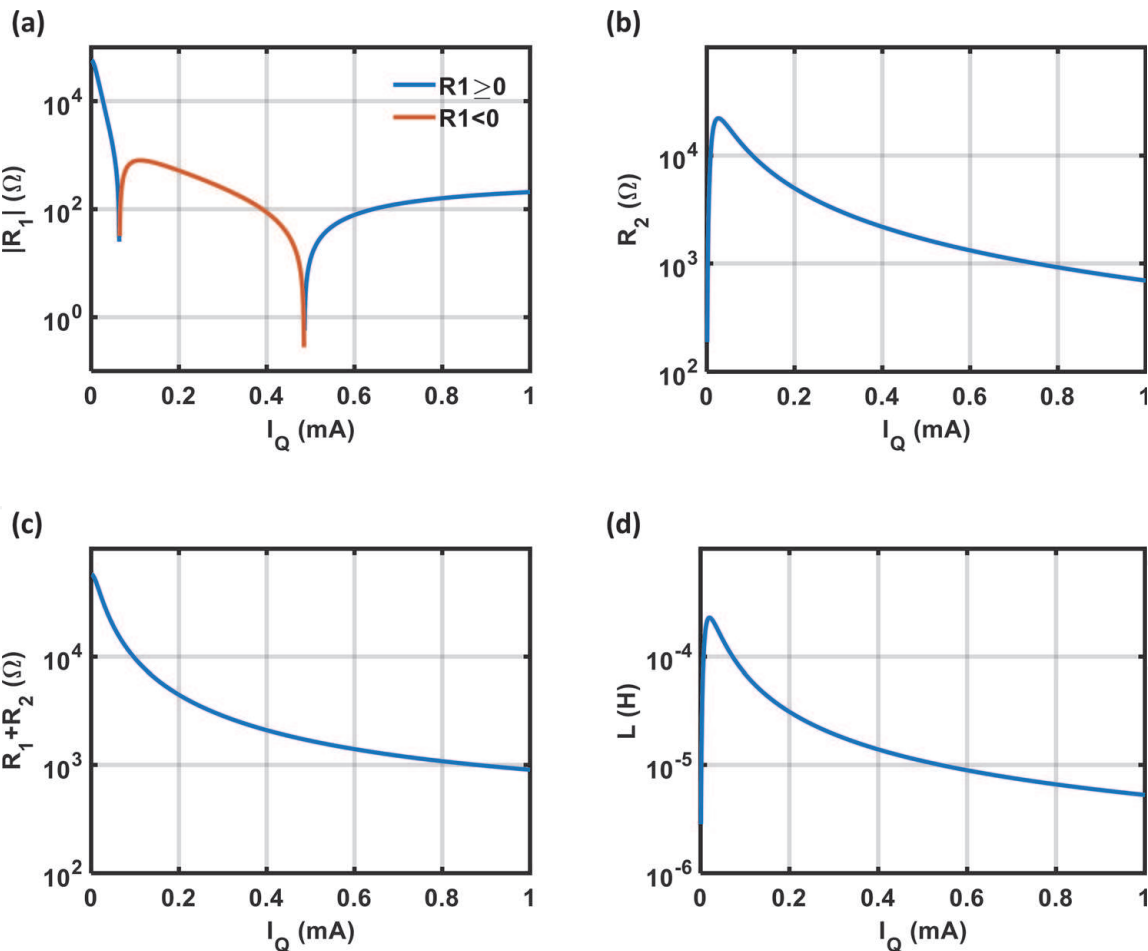

Figure 2.
*Small signal elements values of **Figure 1(b)** are depicted as a function of the DC equilibrium current I_Q, while the parameter values are adopted from **Table 1** during the numerical simulations. (a) $|R_1|$ vs. DC current where positive values of R_1 are depicted in blue color and negative values of R_1 are depicted in orange color. The orange part of $|R_1|$ curve one-to-one corresponds to the NDR region of the DC I-V curve. (b) R_2 vs. I_Q where R_2 always gets positive values. (c) $(R_1 + R_2)$ vs. I_Q. $(R_1 + R_2)$ corresponds to the instantaneous resistance $V(T_o)/I(T_o)$ of the memristor and always gets positive values. (d) L vs. I_Q where L represents the dynamics of the memristor and takes positive values for all current values.*

3. The single cell

To achieve a compact single cell design, a basic solution is to establish oscillatory dynamics by implementing a minimal second-order system accompanied by a simple bias circuitry. Since the memristor itself implements a first-order system with inductive dynamics, an efficient solution to increase the order of the system would be to include an additional capacitor into the cell design. Additionally, we prefer to realize the proper biasing *via* a DC voltage source and a bias resistor. Consequently, the proposed single cell is depicted in **Figure 3(a)** where V_b is the DC voltage source, R_b is the bias resistor, R_s is the series resistor, and C is the parallel capacitor, while the open circle denotes the coupling node.

3.1 Stability analysis of the single cell

Pattern formation through a RD-MCNN prerequisites stable single-cell dynamics in the isolated case. Therefore, in this section, we perform a parametric stability analysis for the uncoupled single cell, which is also the first step of parameter extraction of the circuit element values. A straightforward procedure of stability analysis would require performing linearity analysis on the state equations of the second-order single cell, followed by the derivation of the eigenvalues, to express the stability conditions [37]. In this work, we present a circuit theoretical approach where we employ the AC equivalent circuit of the single cell, which is depicted in **Figure 3(b)**, and derive the stability conditions for the uncoupled case. Adopting this approach, it is possible to express in an efficient way, the stability conditions of the isolated cell in terms of linear circuit element values and of AC element values of the memristor in a parametric form, which enables a direct evaluation of the results. Finally, although the results to be derived should hold for any equilibrium point on the DC I-V curve, without loss of generality, we assume that the memristor is biased in the NDR region, where $R_1 < 0$ and the device is locally active, which is essential for the emergence of complexity.

To derive the stability conditions of the single-cell circuit in **Figure 3(a)**, we firstly obtain the AC equivalent of it, simply by replacing the memristor with its small-signal equivalent (previously introduced in **Figure 1(b)**) and by assuming the DC voltage source as a short-circuit element, resulting in the circuit given in **Figure 3(b)**. Second, we calculate the impedance function $Z(s)$, which is illustrated in **Figure 3(b)**, and given in (3). Here, we would like to note that the poles of $Z(s)$ directly correspond to the eigenvalues of the state equations of the single cell.
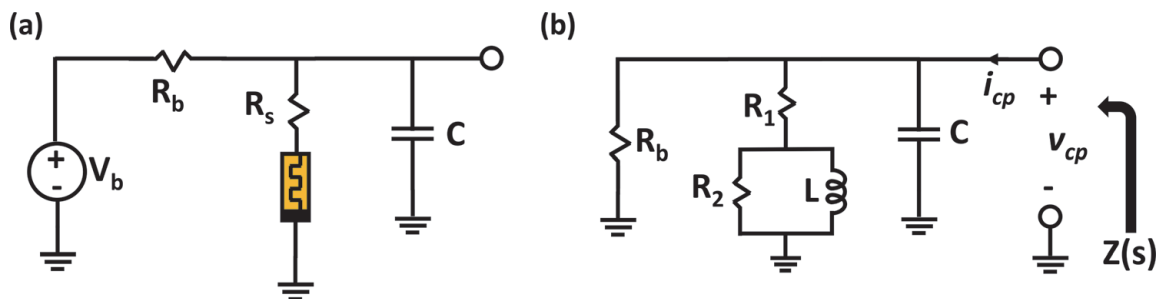

Figure 3.
(a) The single cell of the RD-MCNN structure. V_b is the DC voltage source, R_b is the bias resistor, R_s is the series resistor, C is the parallel capacitor. The open circle denotes the coupling node. (b) AC equivalent of the circuit in (a). The small-signal transfer function $Z(s)$ is the impedance seen through the coupling node.

$$Z(s) = \frac{sL(R_1 + R_2)R_b + R_1R_2R_b}{s^2LC(R_1 + R_2)R_b + s[L(R_1 + R_2 + R_b) + R_1R_2R_bC] + (R_1 + R_b)R_2} = \frac{N(s)}{D(s)}$$

(3)

The stability of $Z(s)$ can be determined by examining the location of the poles of $Z(s)$, or equivalently, the roots of $D(s)$ via Routh-Hurwitz criteria. At this point, it is timely to recall from **Figure 2** that $L > 0$, $R_2 > 0$, and $(R_1 + R_2) > 0$, which reveals the fact that the coefficient of the s^2 term of $D(s)$ is readily positive. Consequently, to guarantee the (asymptotic) stability of $Z(s)$, remaining the coefficients of the $D(s)$ polynomial have to be nonnegative, as dictated by Routh-Hurwitz criteria. Therefore, we have $(R_1 + R_b) > 0$ and $L(R_1 + R_2 + R_b) + R_1R_2R_bC > 0$ that respectively imply that the bias resistor R_b has to be larger than the magnitude of the inverse of the slope of the DC I-V curve (i.e., $R_b > |R_1|$), while C has to be smaller than a critical C_{max} value, which is given in Eq. (4). Here, we would like to note that $D(s)$ would simplify in the absence of the parallel capacitor C, while the first stability condition $(R_1 + R_b) > 0$ would remain the same, as shown in [38], but Eq. (4) would be unnecessary.

$$C < \frac{L(R_1 + R_2 + R_b)}{-R_1R_2R_b} = C_{max}$$

(4)

In **Figure 4(a)**, C_{max} is shown (in blue) as a function of the equilibrium point of the memristor current I_{Q-NDR} across the entire NDR region, for two different values of R_b. It can be seen from **Figure 4(a)** that the smaller value of R_b results in a larger value for C_{max}, which would be beneficial during a hardware realization, while we remind that R_b should be kept larger than $|R_1|$ for a stable operation.

3.2 Local activity analysis of the single cell

The small-signal behavior of an uncoupled cell, which is biased at a locally passive operating point, can be represented by a positive real complexity function (or similarly, by a positive real transfer function for the 1-port coupling case). Subsequently, the AC equivalent circuit of the same cell at the given operating point would be strictly composed of passive linear elements, which inherently results in stable dynamics. Therefore, a diffusive coupling (i.e., the coupling established *via* a resistor) obtained between these identical cells would similarly result in an
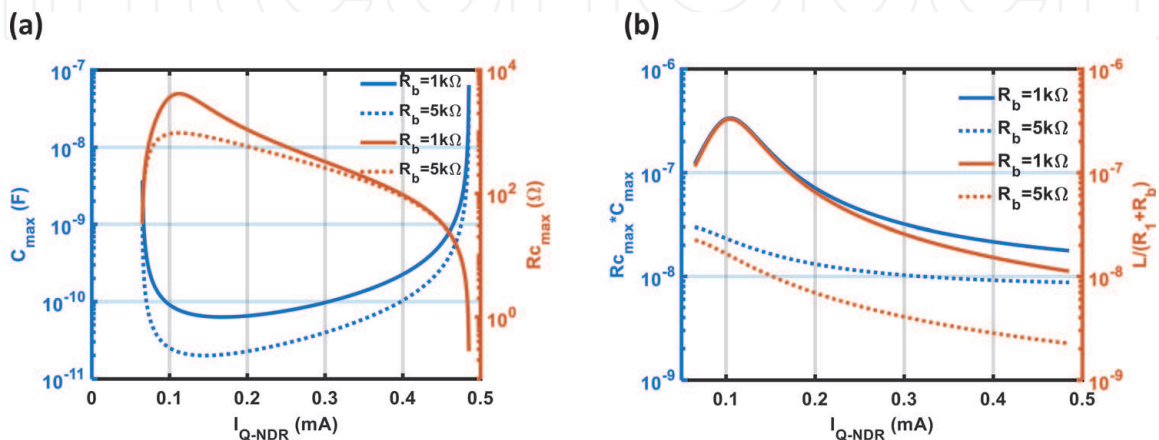

Figure 4.
(a) C_{max} vs. I_{Q-NDR} (blue curves) and R_{c-max} vs. I_{Q-NDR} (orange curves). (b) $C_{max} * R_{c-max}$ product. It can be seen from both graphs that smaller values of R_b results in larger values for C_{max}, R_{c-max}, and $C_{max} * R_{c-max}$ values, while the last product term is more influenced from R_b value.

eventually stable structure since the combination of passive circuit elements through a resistive coupling cannot give rise to instability. Thus, to be able to observe the emergence of complexity in a diffusively coupled homogenous network, it is vital to accommodate locally active cells, which cannot be represented by positive real complexity functions in the small-signal regime. This fact at the same time implies that local activity can be simply judged as a violation of local passivity [9]. Furthermore, a locally active cell is defined to be on the edge-of-chaos, if it is biased at an asymptotically stable operating point. Most importantly, an uncoupled cell, which is poised on the edge-of-chaos and therefore considered as a "dead" or "silent" cell due to its stability, can be potentially destabilized from its quite state *via* resistive coupling, which leads to the generation of complex patterns across the homogenous medium. Correspondingly, the edge-of-chaos domain involves a subset called the sharp-edge-of-chaos domain, which defines the set of parameters that destabilize the cell after coupling is introduced. Strictly speaking, a one-port cell is said to be locally active if and only if its small-signal transfer function (e.g., $Z(s)$ given by Eq. (3) in our case) satisfies any of the conditions below [9]:

1. $Z(s)$ has a pole with positive real part, that is, $Re\,[s] > 0$.

2. $Z(s)$ has multiple poles on the *imaginary* $(j\omega)$ axis.

3. $Z(s)$ has a simple pole $s = j\omega_p$ on the *imaginary* axis and the residue associated with this pole, specifically $r(\,j\omega_p) = \lim\limits_{s \to j\omega_p} Z(s) \bullet (s - j\omega_p)$, is either a negative real number or a complex number.

4. $Re\,[Z(j\omega)] < 0$ for some $\omega \in (-\infty, \infty)$.

To confirm the locally active dynamics of the complexity function $Z(s)$ of Eq. (3), which is associated with the uncoupled cell of **Figure 3(a)**, a direct approach would be to check whether these four rigorously defined criteria are satisfied or not, an approach we had applied in a previous work [28]. However, in this work, we apply a quick inspection method of local activity criteria, and rather check if $Z(s)$ clearly violates local passivity. In consistent with this approach, it can be seen that $Z(s)$ possesses a right half plane (RHP) zero (i.e., $z = -R_1 R_2 / L(R_1 + R_2)$ > 0, for $R_1 < 0$), a feature that cannot be realized with any locally passive transfer function. Thus, without a need for a further examination, we can infer that once it is biased in the NDR region, the uncoupled cell operates in the locally active regime. Furthermore, since the uncoupled cell is designed to be asymptotically stable (*via* tuning R_b and C accordingly), we can directly conclude that it is both locally active and on the edge-of-chaos across the entire NDR region. Finally, we would like to note that the RHP zero is a strong indicator of a possible destabilization scenario after the coupling is established.

3.3 Destabilization analysis after the introduction of coupling

For the emergence of pattern formation, it is essential that the identical cells lose stability after the resistive coupling is established between them. In the previous section, we have studied the stability of the uncoupled cell, while in this section, we investigate the destabilization process after a resistive array is added to couple the elements of the network. Since a direct stability analysis that requires exploring the complete network itself would be complicated and time-consuming, it would be beneficial to apply a simplified stability analysis. Considering highly accurate

illustrative examples, the stability analysis of two-cell [37] and three-cell [29] arrays can be found in the literature. In this work, we present a quick inspection method, which is conceptually introduced in [9] and has been implemented through an example in [28], where the idea is to terminate the coupling node of the single cell with a coupling resistor, resulting in the circuit depicted in **Figure 5(a)** for the case study presented here.

To investigate the possible destabilization scenarios of the resistively terminated cell in **Figure 5(a)**, we follow the same circuit theoretical approach as in the previous subsections and examine the corresponding AC equivalent circuit, which is shown in **Figure 5(b)**. Here, the poles of the impedance function $Z_c(s)$ coincide with the eigenvalues of the second-order system equivalent of the circuit in **Figure 5(a)** at a given equilibrium point and should be examined to determine the destabilization conditions. At this point, it should be noted that the AC equivalent circuits depicted in **Figures 3(b)** and **5(b)** are qualitatively equivalent to each other, while R_c appears additionally in parallel with R_b in **Figure 5(b)**. Therefore, the expression of $Z_c(s)$, readily given in Eq. (5), is identical to the expression of $Z(s)$, where the term R_b is replaced with the parallel equivalent term R_{bc}, that is, $R_{bc} = R_b \bullet R_c/(R_b + R_c)$.

$$Z_c(s) = \frac{sL(R_1 + R_2)R_{bc} + R_1R_2R_{bc}}{s^2LC(R_1 + R_2)R_{bc} + s[L(R_1 + R_2 + R_{bc}) + R_1R_2R_{bc}C] + (R_1 + R_{bc})R_2} = \frac{N_c(s)}{D_c(s)}$$

(5)

To claim instability of $Z_c(s)$, at least one coefficient of the $D_c(s)$ polynomial has to be negative, as dictated by Routh-Hurwitz criteria. Here, it is straightforward to see that the coefficient of the s^2 term of $D_c(s)$ is readily positive. Similarly, it is possible to show after some algebraic rearrangement that the coefficient of the s term remains positive as long as the stability precondition given by Eq. (4), with R_b replaced by R_{bc}, is satisfied. Thus, for instability, the constant term of $D_c(s)$, namely $(R_1 + R_{bc}) \bullet R_2$, has to be negative. Starting with the inequality $(R_1 + R_{bc}) \bullet R_2 < 0$ and replacing R_{bc} with $R_b \bullet R_c/(R_b + R_c)$ directly give us the destabilization condition introduced by Eq. (6).

$$R_c < -\frac{R_1 \bullet R_b}{R_1 + R_b} = R_{c-max} = -(R_1 \| R_b)$$

(6)

In **Figure 4(a)**, we plot (in orange) R_{c-max} as a function of the equilibrium point of the memristor current I_{Q-NDR} across the entire NDR region, for two different values of R_b. Similar to the characteristics of C_{max}, the smaller value of R_b results in a larger value for R_{c-max}, which would relieve the design constraints for an

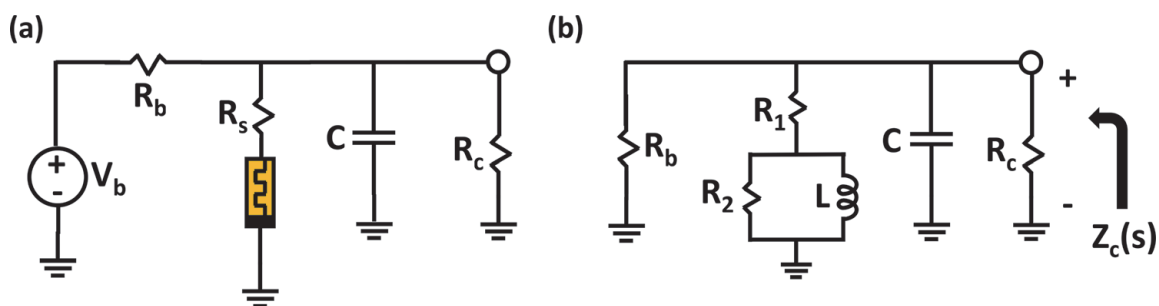(a)   (b)

Figure 5.
(a) A simplified scenario for the resistively coupled single cell where R_c stands for the coupling resistor. (b) AC equivalent circuit of the cell in (a). The poles of $Z_c(s)$ shall be investigated for analyzing the stability of the circuit in (a) at a given equilibrium point.

hardware realization. On the other hand, Eq. (6) reveals the fact that considering the memristor model-dependent quantities, R_{c-max} depends only on the slope of the I-V curve (i.e., R_1^{-1}), while C_{max} depends on other quantities (see Eq. (4)) as well. Besides, as a function of I_{Q-NDR}, the characteristics of C_{max} increase (decrements), while the characteristics of R_{c-max} decrease (increments). Moreover, it is interesting to mention that the condition derived in Eq. (6) is qualitatively equivalent to the results presented in [29, 37], indicating the fact that the simplification considered in this work is accurate and provides a quick insight into the destabilization scenario of the coupled cell in **Figure 5(a)**.

Considering a typical time constant based design approach, we characterize the term $R_{c-max} \bullet C_{max}$, introducing the exact and an approximate product in Eq. (7), and plot these quantities in **Figure 4(b)** as a function of I_{Q-NDR}, for two different values of R_b. Here, we would like to note that the approximate product term $L/(R_1 + R_b)$ is obtained under the assumption $(R_1 + R_2 + R_b) \cong R_2$.

$$R_{c-max} \bullet C_{max} = -\frac{R_1 \bullet R_b}{R_1 + R_b} \bullet \frac{L(R_1 + R_2 + R_b)}{-R_1 R_2 R_b} = \frac{L(R_1 + R_2 + R_b)}{R_2(R_1 + R_b)} \cong \frac{L}{(R_1 + R_b)} \quad (7)$$

It can be seen from **Figure 4(b)** that the approximated time constant term given in Eq. (7) follows the original expression very closely, especially for the smaller value of R_b. Moreover, the approximated value is independent of R_2, but rather dependent on the dynamic quantity L, or in other words, the switching speed of the memristor device. As a final and crucial remark, referring to the instability region of parameters, that is, the sharp-edge-of-chaos domain, it is possible to rigorously define the necessary circuit design variables by taking into account the parametric equations given by Eqs. (4) and (6).

4. RD-MCNN structure and static pattern formation

The proposed RD-MCNN structure has a planar grid arrangement and it is composed of $m \times n$ identical cells where m is the number of rows, n is the number of columns, and $C_{i,j}$ represents the cell at i^{th} row and the jth column. All the cells are resistively coupled to the respective nearest neighbors in vertical and horizontal directions only, and the CNN structure assumes periodic boundary conditions; that is, the first and the last cells in each row, and respectively, in each column, are resistively coupled to each other as well. To study the emergence of pattern formation dynamics in the proposed RD-MCNN, among several structures investigated, here we present typical simulation results of a two-dimensional 51×51 structure. We define the same initial conditions ($T_0 = 300K$ and $V_{c0} = 0V$) for all the cells unless otherwise stated, except for the cell, namely $C_{26,26}$, which is in the center of the network. This exception for the definition of initial conditions is adopted to initiate the emergence of the transient behavior in the numerical simulations.

First of all, we investigate the effect of changing the DC operating point on the static pattern formation. To this end, we set the design parameters R_b to $2k\Omega$ and R_c to $0.1k\Omega$, while we tune V_b to vary the location of the DC operating point of each cell. We present the emergent static patterns in **Figure 6**, where $V_b = 1.2V$ in **Figure 6(a)**, $V_b = 1.3V$ in **Figure 6(b)**, $V_b = 1.4V$ in **Figure 6(c)**, and $V_b = 1.5V$ in **Figure 6(d)**. Here, we plot the memristor voltage, or equivalently, the capacitor voltage, of each cell and assign a color code to its amplitude value, as depicted on the right side of each plot. It is possible to observe from **Figure 6** that a shift in the location of the operating point due to an increase in V_b may lead to static patterns featuring a reduced spread in capacitor voltage amplitude through the array,
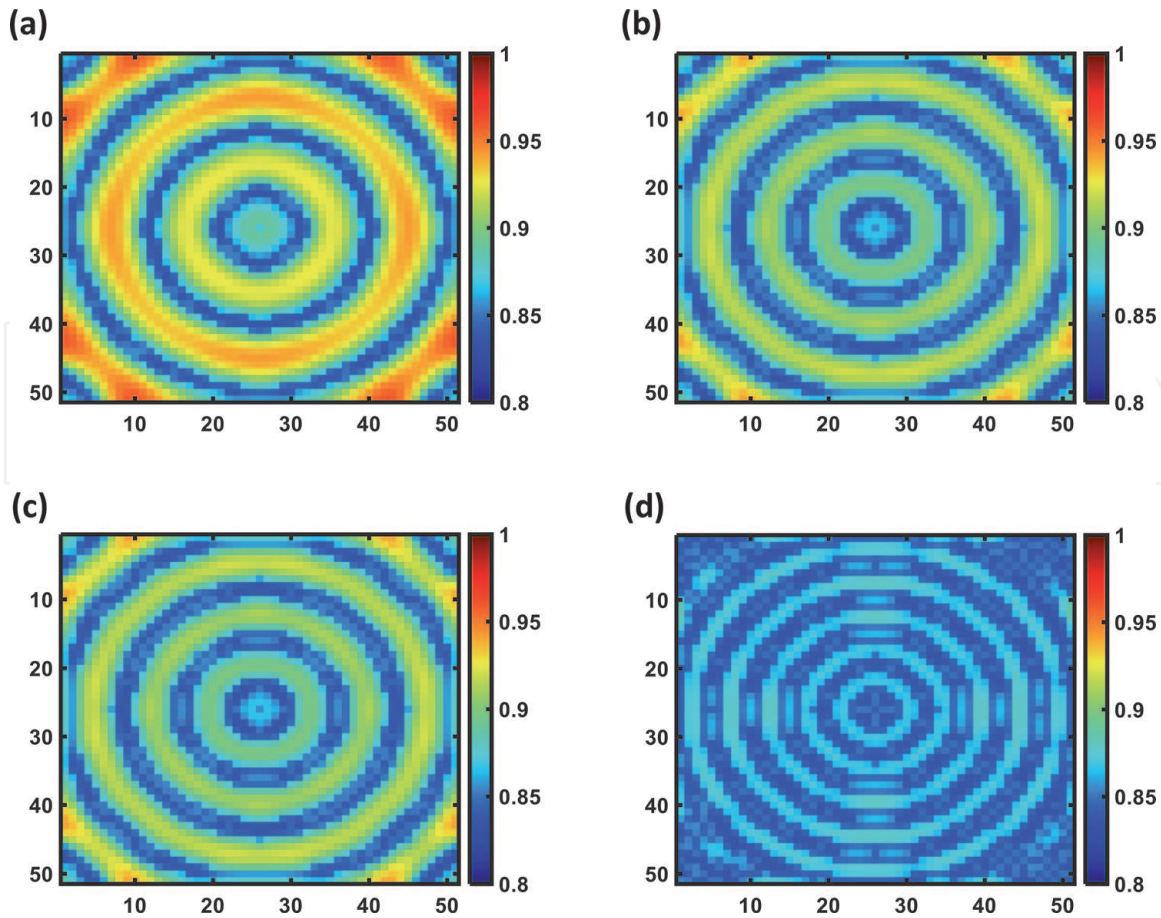
Figure 6.
RD-MCNN output values represented by the cell memristor voltages obtained in a simulation of a two-dimensional 51×51 RD-MCNN structure for $R_b = 2k\Omega$, $R_c = 0.1k\Omega$, while $V_b = 1.2V$ in (a), $V_b = 1.3V$ in (b), $V_b = 1.4V$ in (c), and $V_b = 1.5V$ in (d). All the cells have the same initial conditions except for the center cell $C_{26,26}$. A shift in the memristor DC operating point may lead to static patterns with a reduced range in capacitor voltage amplitude, as mostly pronounced in (d).

reflected by a gradual decrement in the variety of colors in the emergent patterns, as especially observed in **Figure 6(d)**.

Later on, we examine the effect of the coupling strength on the static pattern formation by varying the value of the coupling resistance R_c. Similarly, we set the design parameters V_b to $1.2V$ and R_b to $2k\Omega$ while we tune the value of R_c to adjust the coupling strength. The results are illustrated in **Figure 7**, where $R_c = 0.25k\Omega$ in **Figure 7(a)**, $R_c = 0.5k\Omega$ in **Figure 7(b)**, $R_c = 1k\Omega$ in **Figure 7(c)**, and $R_c = 2k\Omega$ in **Figure 7(d)**. It can be seen that as R_c increases, first a deformation starts to occur in the outer parts of the static pattern of **Figure 7(a)–(c)**, while clearly, a new static pattern emerges, finally in **Figure 7(d)**. The final pattern in **Figure 7(d)** also shows that neighboring cells exhibit a sharper spread in the capacitor voltage amplitude, which is reflected by the clear color contrast observable in this plot, especially as compared to that of **Figure 7(a)**.

In addition, we focus on the effect of the initial conditions on pattern formation, as depicted in **Figure 8**, where we fix the values of all of the design parameters such that $V_b = 1.2V$, $R_b = 2k\Omega$, and $R_c = 0.1k\Omega$. The cells located in the center of each side of the edges (i.e., $C_{1,26}$, $C_{26,1}$, $C_{51,26}$, $C_{26,51}$), or midpoint cells for short, have the same initial condition as the center cell $C_{26,26}$ in **Figure 8(a)**, while only the corner cells ($C_{1,1}$, $C_{1,51}$, $C_{51,1}$, $C_{51,51}$) have the same initial condition as the center cell $C_{26,26}$ in **Figure 8(c)**. On the other hand, only the midpoint cells share the same initial conditions in **Figure 8(b)**, while the center cell $C_{26,26}$ features the same initial condition as the rest of the network. Similarly, only the corner cells share the same
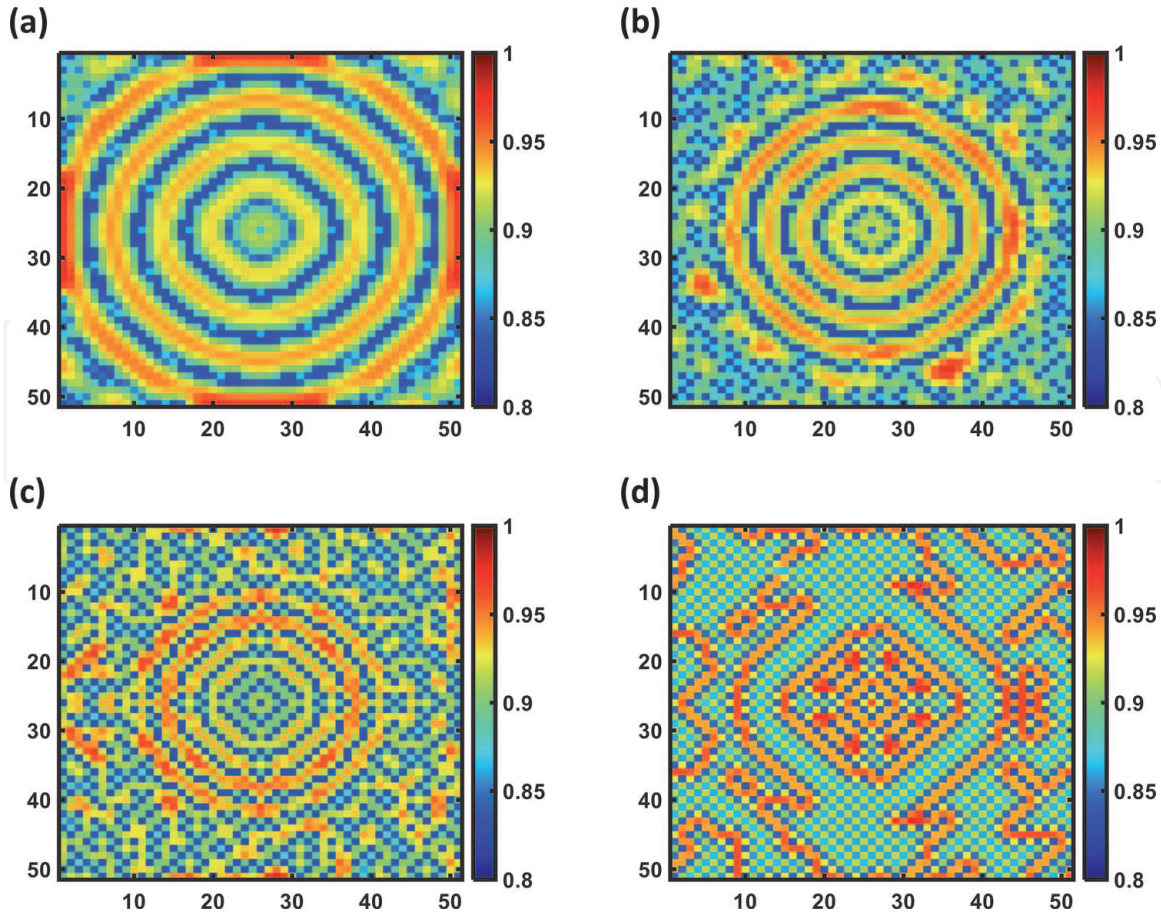
Figure 7.
RD-MCNN output values represented by the cell memristor voltages obtained in a simulation of a two-dimensional 51×51 RD-MCNN structure for $R_b = 2k\Omega$, $V_b = 1.2V$, while $R_c = 0.25k\Omega$ in (a), $R_c = 0.5k\Omega$ in (b), $R_c = 1k\Omega$ in (c), and $R_c = 2k\Omega$ in (d). All the cells have the same initial condition except for the center cell $C_{26,26}$. As R_c increases, first a deformation occurs in the outer parts of the pattern observed in (a), as shown in (b) and (c), while a clearly new pattern emerges in (d). With reference to the pattern in (d), the capacitor voltages in neighboring cells exhibit a sharper change in the amplitude, which is practically reflected by the color contrast observable, especially as compared to that of (a).

initial conditions in **Figure 8(d)**, while the center cell $C_{26,26}$ features the same initial condition as the rest of the network cells. The difference between the patterns presented in **Figure 8(a)** and **(b)**, and equivalently in **Figure 8(c)** and **(d)**, shows the effect of a change in the number of cells sharing the same initial conditions. Likewise, the difference between the patterns presented in **Figure 8(a)** and **(c)**, and equivalently in **Figure 8(b)** and **(d)**, shows the effect of a change in the location (indeed, a rotation of half-side length) of cells sharing the same initial conditions, which can result in clearly different patterns. Since there exists a very high number of spatial permutations for the location and the number of cells with the same initial conditions, we conjecture that there may appear a large class of clearly distinguishable patterns, such as those presented in **Figure 8**, which results in a significant memory capacity of the network.

Lastly, we investigate the effect of the size of the network on the patterns generated through. For this purpose, we set the design parameters V_b to $1.2V$, R_b to $2k\Omega$, and R_c to $0.2k\Omega$, while we define the same initial conditions for the corner cells as it is the case for the center cell. Then, we simulate structures of different size while preserving their square geometry, and depict the results in **Figure 9**, where $m = n = 31$ in **Figure 9(a)**, $m = n = 41$ in **Figure 9(b)**, $m = n = 51$ in **Figure 9(c)**, and $m = n = 61$ in **Figure 9(d)**. Once more, it can be concluded from **Figure 9** that the patterns generated across networks of different sizes and square geometry are clearly distinguishable one from the other.
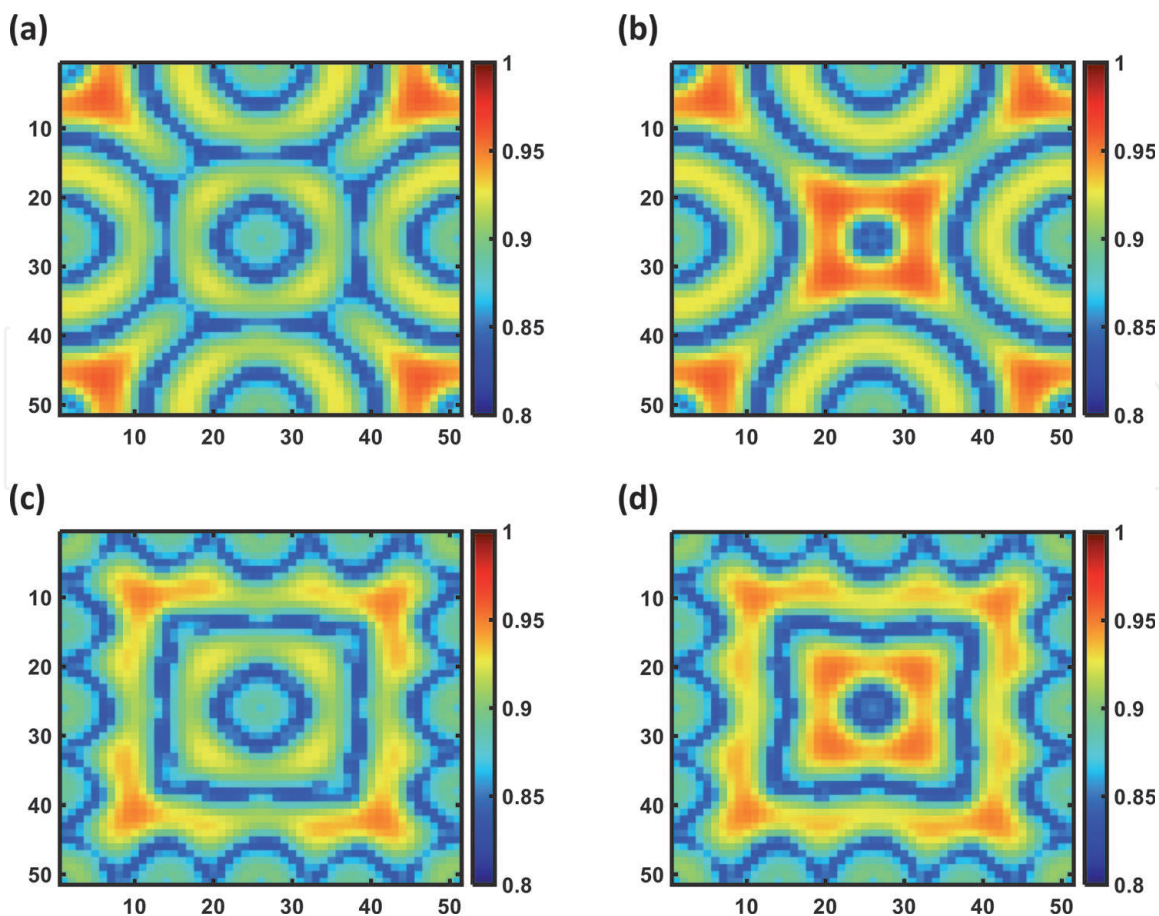
Figure 8.
RD-MCNN output values represented by the cell memristor voltages obtained in a simulation of a two-dimensional 51×51 RD-MCNN structure for $R_b = 2k\Omega$, $R_c = 0.1k\Omega$ and $V_b = 1.2V$. The cells in the middle of each side of the edges, or briefly the midpoint cells ($C_{1,26}, C_{26,1}, C_{51,26}, C_{26,51}$), have the same initial conditions as the center cell $C_{26,26}$ in (a), while the corner cells ($C_{1,1}, C_{1,51}, C_{51,1}, C_{51,51}$) have the same initial conditions as the center cell $C_{26,26}$ in (c). On the other hand, only the midpoint cells share the same initial conditions in (b), while the center cell $C_{26,26}$ features the same initial condition as the rest of the network cells. Similarly, only corner cells share the same initial conditions in (d), while the center cell $C_{26,26}$ features the same initial conditions as the rest of the network cells. A change in the location as well as in the number of cells sharing the same initial conditions can result in clearly different patterns, conferring the network a significant memory capacity.

5. Conclusion

In this chapter, we have presented the mathematical investigation of static pattern formation across a resistively coupled RD-MCNN structure *via* the application of the theory of local activity. The considered networks have identical cells in a compact form, each of which is composed of a DC bias voltage source, a bias resistor, a locally active memristor, and a parallel capacitor. The memristor was represented through a generic model, which helped to reduce the numerical complexity and to shorten the simulation time of large-scale networks. A useful AC equivalent circuit could be derived for the locally active device, which facilitated further calculations related to the small signal model of the network cell. We have adopted a systematic circuit theoretical approach that we applied for the stability analysis of the isolated cell and for the extraction of its parameter values for its operation on the edge-of-chaos and sharp-edge-of-chaos domains. In this way, we have performed a simple, fast, and robust analysis, which at the same time allowed an efficient interpretation of the results. All the calculations were performed in parametric form, which allowed a deep investigation of the results, making it possible to extract the related sets of parameters in terms of the cell characteristics, namely the DC operating point and the capacitor value, as well as the value of the
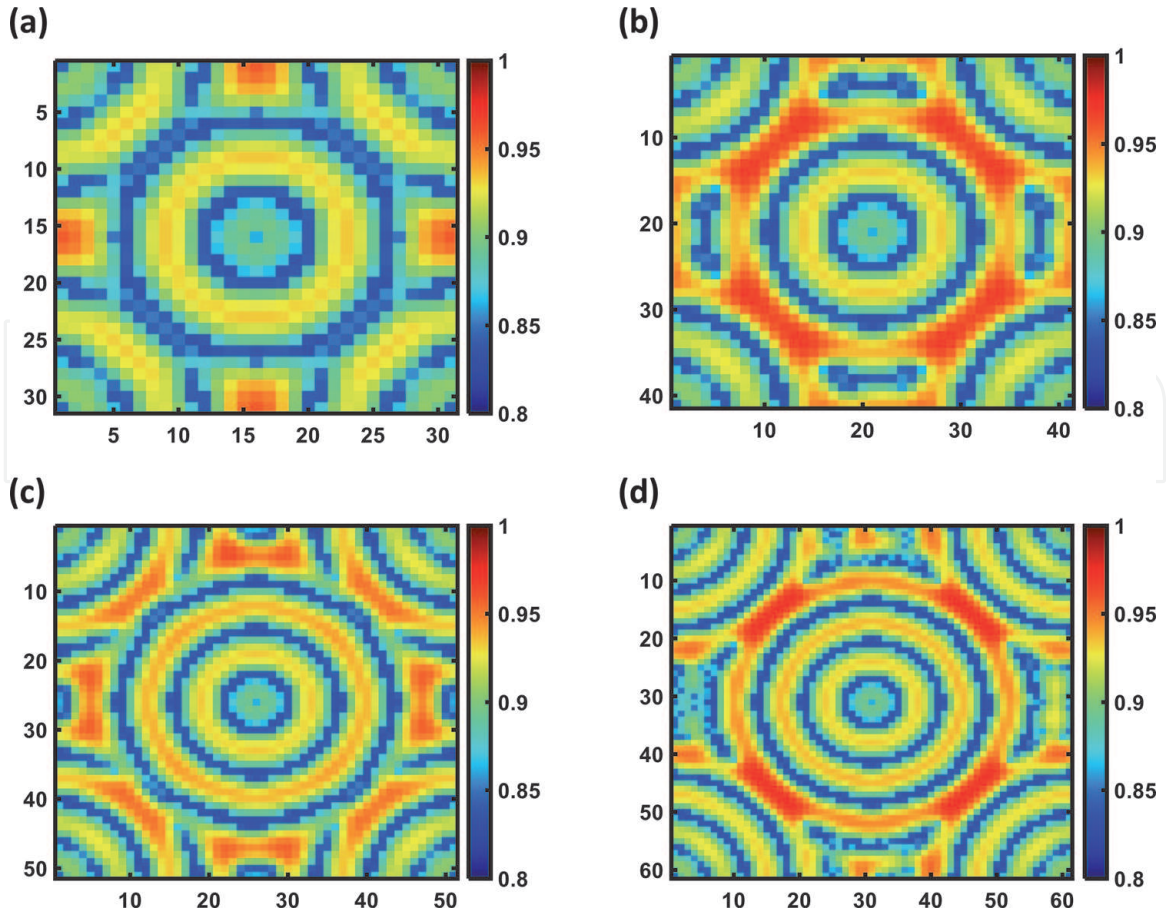
Figure 9.
Simulation results of various $m \times n$ RD-MCNN structures for $R_b = 2k\Omega$, $R_c = 0.2k\Omega$ and $V_b = 1.2V$, where $m = n = 31$ in (a), $m = n = 41$ in (b), $m = n = 51$ in (c), and $m = n = 61$ in (d). The corner cells have the same initial conditions as the center cell for all the structures. Although the four structures share a square geometry, they differ in size, which leads to clearly distinguishable patterns.

coupling resistance. The proposed RD-MCNN was shown to generate diverse patterns while we have extensively investigated the effect of design parameters, initial conditions, and the size of the network on the patterns generated therein. Furthermore, the mathematical and circuit theoretical approach employed during the investigation of pattern formation dynamics in the RD-MCNN under focus in this chapter can be easily adopted to RD-MCNNs with different cell designs.

Finally, the content of this work can be extended to the investigation of the role of the network geometry and variety in cells' initial conditions on pattern formation. Furthermore, the impact of memristor non-idealities such as variability in memristor behavior from cycle to cycle, as well as from device to device, and endurance degradation and short- and long-term reliability issues shall be further examined to achieve a robust design. Such non-idealities, essentially, can affect the NDR characteristics of the memristors and narrow the width of the NDR region, or the devices can even get stuck in one of the high-resistance or low-resistance locally passive regimes where they act as dead cells without any dynamics. Preliminary simulation results show that endowing memristors with narrower NDR width negatively affect the patterns' color contrasts, while the presence of the high- or low-resistance locally passive devices results in the formation of color clusters within the patterns. Interestingly, similar color clusters emerge also when some of the array memristors' initial conditions are randomly selected, which suggests a possible strategy to compensate for the disturbing action of locally passive cells on the formation of predefined patterns through a dynamic conditioning of their initial conditions. Similarly, the low color contrast quality in the patterns, which occur due

to the existence of memristors featuring a narrower NDR region, can be improved by reprogramming dynamically the bias voltage sources in these "defect" cells. In conclusion, proper control strategies including cells' dynamic biasing and initial condition conditioning, as well as reconfiguration of the network array, may be considered as a solution to overcome the harmful effects which memristor non-idealities may induce on the emergence of predefined patterns in the proposed RD-MCNNs. Future studies will also be devoted to envision an application, where the capability of our cellular medium to generate a variety of steady-state static patterns may be useful to our modern society.

Acknowledgements

Author details

Ahmet Samil Demirkol*, Alon Ascoli, Ioannis Messaris and Ronald Tetzlaff
Technische Universität Dresden (TUD), Dresden, Germany

*Address all correspondence to: ahmet_samil.demirkol@tu-dresden.de

IntechOpen

References

[1] Walgraef D. Spatio-Temporal Pattern Formation with Examples from Physics, Chemistry, and Materials Science. NY: Springer-Verlag; 1997. p. 306. DOI: 10.1007/978-1-4612-1850-0

[2] Maini PK, Painter KJ, Chau HNP. Spatial pattern formation in chemical and biological systems. Journal of the Chemical Society, Faraday Transactions. 1997;**93**(20):3601-3610. DOI: 10.1039/A702602A

[3] Demir E, Yaman IY, Basaran M, Kocabas A. Dynamics of pattern formation and emergence of swarming in *Caenorhabditis elegans*. eLife. 2020;**9**: 1-21. DOI: 10.7554/eLife.52781

[4] Shao X, Wilson P, Saylor J, Bostwick J. Surface wave pattern formation in a cylindrical container. Journal of Fluid Mechanics. 2021;**915**: A19. DOI: 10.1017/jfm.2021.97

[5] Meakin P, Jamtveit B. Geological pattern formation by growth and dissolution in aqueous systems. Proceedings of the Royal Society A. 2010;**466**:659-694. DOI: 10.1098/rspa.2009.0189

[6] Hutt MT, Kaiser M, Hilgetag CC. Perspective: Network-guided pattern formation of neural dynamics. Philosophical Transactions of the Royal Society B. 2014;**369**:20130522. DOI: 10.1098/rstb.2013.0522

[7] Turing AM. The chemical basis of morphogenesis. Philosophical Transactions. Royal Society of London. 1952;**B237**:37-72. DOI: 10.1098/rstb.1952.0012

[8] Sekimura T, Noji S, Ueno N, Maini PK, editors. Morphogenesis and Pattern Formation in Biological Systems. Japan: Springer; 2003. p. 398. DOI: 10.1007/978-4-431-65958-7

[9] Chua L. Local activity is the origin of complexity. International Journal of Bifurcation and Chaos. 2005;**15**(11): 3435-3456. DOI: 10.1142/S0218127405014337

[10] Slavova A, Tetzlaff R. Mathematical analysis of memristor CNN, memristors. In: James A, editor. Circuits and Applications of Memristor Devices. IntechOpen. 2019. DOI: 10.5772/intechopen.86446

[11] Gilli M, Roska T, Chua L, Civalleri PP. On the relationship between CNNs and PDEs. In: Proc. of the 7th IEEE Int. Workshop on Cellular Neural Networks and Their App. 24-24 July 2002; Germany: IEEE; 2002. pp. 16-24. DOI:10.1109/CNNA.2002.1035030

[12] Arena P, Fortuna L, Branciforte M. Reaction-diffusion CNN algorithms to generate and control artificial locomotion. IEEE Transactions on Circuits and Systems I: Fundamental Theory and Applications. 1999;**46**(2): 253-260. DOI: 10.1109/81.747195

[13] Chua L. CNN: A Paradigm for Complexity. World Scientific Series on Nonlinear Science Series A. Singapore: World Scientific Publishing Co. Pte. Ltd.; 1998. Vol. 31. p. 332. DOI: 10.1142/3801

[14] Buscarino A, Corradino C, Fortuna L, Frasca M. Turing patterns via pinning control in the simplest memristive cellular nonlinear networks. Chaos: An Interdisciplinary Journal of Nonlinear Science. 2019;**29**:103145. DOI: 10.1063/1.5115131

[15] 5G Evolution and 6G [Internet]. Available from: https://www.nttdoc omo.co.jp/english/binary/pdf/corpora te/technology/whitepaper_6g/DOCOMO_6G_White_PaperEN_20200124.pdf [Accessed: 01 August 2021]

[16] Ielmini D, Wong HSP. In-memory computing with resistive switching devices. Nature Electronics. 2018;**1**: 333-343. DOI: 10.1038/s41928-018-0092-2

[17] Slesazeck S, Mikolajick T. Nanoscale resistive switching memory devices: A review. Nanotechnology. 2019;**30**: 352003. DOI: 10.1088/1361-6528/ab2084

[18] Chua L. Memristor—The missing circuit element. IEEE Transactions on Circuit Theory. 1971;**18**(5):507-519. DOI: 10.1109/TCT.1971.1083337

[19] Chua L. Everything you wish to know about memristors but are afraid to ask. Radioengineering. 2015;**24**(2): 319-368. DOI: 10.13164/re.2015.0319

[20] Pickett M, Medeiros-Ribeiro G, Williams RS. A scalable neuristor built with Mott memristors. Nature Materials. 2013;**12**:114-117. DOI: 10.1038/nmat3510

[21] Xia Q, Yang JJ. Memristive crossbar arrays for brain-inspired computing. Nature Materials. 2019;**18**:309-323. DOI: 10.1038/s41563-019-0291-x

[22] Tetzlaff R, Ascoli A, Messaris I, Chua L. Theoretical foundations of memristor cellular nonlinear networks: Memcomputing with bistable-like memristors. IEEE Transactions on Circuits and Systems I: Regular Papers. 2020;**67**(2):502-515. DOI: 10.1109/TCSI.2019.2940909

[23] Ascoli A, Messaris I, Tetzlaff R, Chua L. Theoretical foundations of memristor cellular nonlinear networks: Stability analysis with dynamic memristors. IEEE Transactions on Circuits and Systems I: Regular Papers. 2020;**67**(4):1389-1401. DOI: 10.1109/TCSI.2019.2957813

[24] Ascoli A, Tetzlaff R, Kang SM, Chua L. Theoretical foundations of memristor cellular nonlinear networks: A DRM2-based method to design memcomputers with dynamic memristors. IEEE Transactions on Circuits and Systems I: Regular Papers. 2020;**67**(8):2753-2766. DOI: 10.1109/TCSI.2020.2978460

[25] Ascoli A, Tetzlaff R, Kang SM, Chua L. System-theoretic methods for designing bio-inspired mem-computing memristor cellular nonlinear networks. Frontiers in Nanotechnology. 2021;**3**: 633026. DOI: 10.3389/fnano.2021.633026

[26] Buscarino A, Corradino C, Fortuna L, Frasca M, Chua L. Turing patterns in memristive cellular nonlinear networks. IEEE Transactions on Circuits and Systems I: Regular Papers. 2016;**63**(8):1222-1230. DOI: 10.1109/TCSI.2016.2564738

[27] Weiher M, Herzig M, Tetzlaff R, Ascoli A, Mikolajick T, Slesazeck S. Pattern formation with locally active S-type NbOx memristors. IEEE Transactions on Circuits and Systems I: Regular Papers. 2019;**66**(7):2627-2638. DOI: 10.1109/TCSI.2019.2894218

[28] Demirkol AS, Ascoli A, Messaris I, Tetzlaff R. Analytical investigation of pattern formation in an M-CNN with locally active NbOx memristors. In: IEEE International Symposium on Circuits and Systems (ISCAS2021). 2021. pp. 1-5. DOI:10.1109/ISCAS51556.2021.9401280

[29] Demirkol AS, Ascoli A, Tetzlaff R. Mathematical investigation of static pattern formation with a locally active memristor model. In: The 17th IEEE International Workshop on Cellular Nanoscale Networks and their Applications. Catania: CNNA2021 [Accepted for Publication]

[30] Kumar S, Strachan JP, Williams RS. Chaotic dynamics in nanoscale NbO2 Mott memristors for analogue computing. Nature. 2017;**548**:318-321. DOI: 10.1038/nature23307

[31] Herzig M, Weiher M, Ascoli A, Tetzlaff R, Mikolajick T, Slesazeck S. Multiple slopes in the negative differential resistance region of NbOx-based threshold switches. Journal of Physics D: Applied Physics. 2019;**52**: 325104. DOI: 10.1088/1361-6463/ab217a

[32] Messaris I, Tetzlaff R, Ascoli A, Williams RS, Kumar S, Chua L. A simplified model for a NbO2 Mott memristor physical realization. In: IEEE International Symposium on Circuits and Systems (ISCAS); 2020. pp. 1-5. DOI:10.1109/ISCAS45731.2020.9181036

[33] Ascoli A, Demirkol AS, Tetzlaff R, Slesazeck S, Mikolajick T, Chua L. On local activity and edge of chaos in a NaMLab memristor. Frontiers in Neuroscience. 2021;**15**:651452. DOI: 10.3389/fnins.2021.651452

[34] Li S, Liu X, Nandi SK, Nath SK, Elliman RG. Origin of current-controlled negative differential resistance modes and the emergence of composite characteristics with high complexity. Advanced Functional Materials. 2019;**29**(44):1905060. DOI: 10.1002/adfm.201905060

[35] Kuo FF. Network Analysis and Synthesis. Wiley International Edition, Singapore: John Wiley & Sons; 1966. p. 515

[36] Messaris I, Brown T, Demirkol AS, Al Chawa MM, Williams RS, Tetzlaff R, et al. NbO2-Mott memristor: A circuit-theoretic investigation. IEEE Transactions on Circuits and Systems I: Regular Papers. 2021 [Under Review]

[37] Ascoli A, Demirkol AS, Tetzlaff R, Chua L. Edge of chaos theory resolves smale paradox in the simplest memristor oscillatory network. IEEE Transactions on Circuits and Systems I: Regular Papers. 2021 [Under Review]

[38] Ascoli A, Slesazeck S, Mähne H, Tetzlaff R, Mikolajick T. Nonlinear dynamics of a locally-active memristor. IEEE Transactions on Circuits and Systems I: Regular Papers. 2015;**62**(4): 1165-1174. DOI: 10.1109/TCSI.2015.2413152